OPEN ACCESS
IOP Publishing

Semiconductor Science and Technology

Semicond. Sci. Technol. **36** (2021) 025011 (12pp)

https://doi.org/10.1088/1361-6641/abce1b

A comparative study on GaSb epilayers grown on nominal and vicinal Si(100) substrates by molecular beam epitaxy

Burcu Arpapay[1], **Y Eren Suyolcu**[2,3], **Gülcan Çorapçıoğlu**[4,5], **Peter A van Aken**[3], **Mehmet Ali Gülgün**[6] and **Uğur Serincan**[1]

[1] Nanoboyut Research Laboratory, Department of Physics, Faculty of Science, Eskişehir Technical University, Eskişehir, Turkey
[2] Department of Materials Science and Engineering, Cornell University, Ithaca, NY 14853, United States of America
[3] Max Planck Institute for Solid State Research, Heisenbergstrasse 1, Stuttgart 70569, Germany
[4] Central Research Infrastructure Directorate, Koc University, Rumelifeneri Yolu, Sariyer 34450, Istanbul, Turkey
[5] Sabanci University Nanotechnology Research and Application Center, Istanbul 34956, Turkey
[6] Sabanci University, Engineering and Natural Sciences, Istanbul 34956, Turkey

E-mail: barpapay@eskisehir.edu.tr and barpapay@yahoo.com

Received 8 September 2020, revised 22 October 2020
Accepted for publication 26 November 2020
Published 23 December 2020

Abstract

The direct growth of GaSb buffer layers on Si substrates is attracting considerable interest in the integration of group III-Sb based device structures on lower-cost Si substrates. Here, we present the effect of various growth steps on the defect types and defect density that are crucial for advancing high crystal quality GaSb buffer layer on nominal/vicinal Si substrate. As a growth step, the applied thermal annealing at an intermediate step provided a decrease in the threading dislocation (TD) density down to 1.72×10^8 cm^{-2}, indicating a more effective method compared to post-growth annealing. Additionally, the importance of period number and position of GaSb/AlSb superlattice layers inserted in GaSb epilayers is demonstrated. In the case of the GaSb epilayers grown on vicinal substrates, the APB density as low as 0.06 μm^{-1} and TD density of 1.98×10^8 cm^{-2} were obtained for the sample grown on 4° miscut Si(100) substrate.

Supplementary material for this article is available online

Keywords: molecular beam epitaxy, GaSb epilayer, anti-phase boundary, miscut angle, lattice mismatched growth

(Some figures may appear in colour only in the online journal)

1. Introduction

The combination of outstanding characteristics of group III–V compounds and Si has received much attention for fabrication of functional semiconductor devices in recent years [1–3]. This will pave the way for manufacturing not only the cost-effective but also high-speed optoelectronic devices. Si is traditionally known as the raw material used in electronic devices. It has widespread applications in semiconductor industry due to its low cost and mature production technology. The main disadvantage of Si is its indirect band gap structure, which limitates the usage of Si in optoelectronic devices. Direct band gap group III–V compounds, on the other hand, provide an efficient solution for optoelectronic and high-speed

Original content from this work may be used under the terms of the Creative Commons Attribution 4.0 licence. Any further distribution of this work must maintain attribution to the author(s) and the title of the work, journal citation and DOI.

 © 2020 The Author(s). Published by IOP Publishing Ltd Printed in the UK

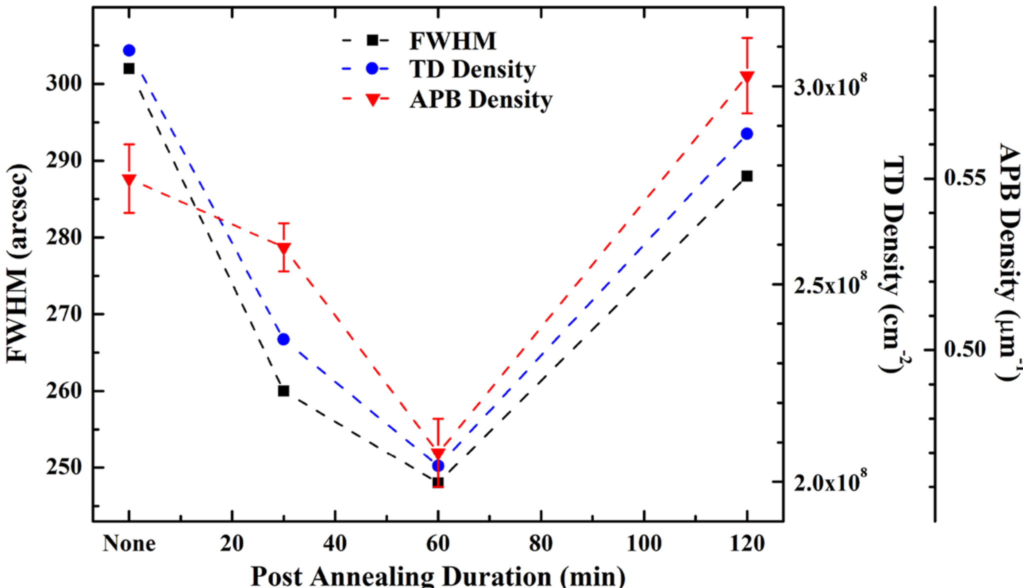

Figure 1. The FWHM of x-ray RC around the (004) reflection, the TD and APB densities of the GaSb epilayers as a function of post-growth annealing duration. The durations none, 30, 60 and 120 min correspond to the samples NB#1, NB#2, NB#3, and NB#4, respectively. The dotted lines are guide for the eyes.

devices. Therefore, the idea of integration of group III–V compounds on Si emerges. However, the main practical challenges in this concept are the large lattice mismatch and thermal expansion coefficient difference between group III–V compounds and Si, as well as the growth of polar group III–V compounds on nonpolar Si. Consequently, misfit dislocations, threading dislocations (TDs), antiphase boundaries (APBs), micro-twins (MTs) and micro-cracks appear during the direct growth of group III–V compounds on Si.

Among group III–V compounds, GaSb is a versatile material for a wide range of applications, especially for infrared photodetectors [4]. However, the main drawback to GaSb substrates is the high-price production cost, which leads us to less expensive substrates such as Si. In the case of integration of Sb-based devices with Si substrates, ∼12% lattice mismatch between GaSb and Si and the corresponding 0.67 monolayer (ML) critical thickness of GaSb on Si [5] become a crucial issue for the growth of a high crystal quality buffer layer directly on Si substrate. Although Sb-based photodetectors on Si have been successfully demonstrated in recent years [6–8], the growth conditions for buffer layers still need to be improved for better device performances.

The challenges in growth of GaSb on Si could be overcome to some extent by using post-annealing treatment, low/high growth temperature combinations, AlSb nucleation layers (NL), superlattice (SL) layers, and Si substrates with various miscut angles [9–14]. The initial growth of the AlSb NL on Si reduces crystal imperfections in GaSb epilayers [9]. Even if AlSb islands act as nucleation sites for Ga and Sb species, and enhance the surface morphology of overlayers, GaSb epilayers still contain TDs and planar defects such as APBs. For the suppression of APBs, originating from the heteroepitaxy of polar group III–V compounds on nonpolar Si substrates, the most common application is the use of vicinal Si(100) substrates deliberately tilted at small angles (0.15°–6°) towards the (110) plane [15]. Other ways of reducing the dislocation density are thermal treatment and insertion of SL layers [16, 17]. Thus, it is crucial to reduce the density of defects with applied growth steps and investigate their limitations. In our previous study, utilizing a defect sensitive solution, we successfully demonstrated the existence of APBs, MTs, and etch pits on the surface of the GaSb epilayers grown on nominal Si(100) substrates [18]. To the best of our knowledge, a comparative study about the structural analysis of GaSb epilayers grown on nominal and vicinal Si(100) substrates by using molecular beam epitaxy (MBE) has not been reported yet.

Table 1. Summary of the obtained results from the samples NB#1 and NB#2.

Sample code	NB#1[a]	NB#2
RC FWHM (arcsec)	302	260
TD density (cm^{-2})	3.09×10^8	2.36×10^8
The APB density (μm^{-1})	0.55	0.53
RMS (nm)	1.06	1.20

[a] Reference sample.

For further improvement in highly mismatched GaSb on Si, it is essential to figure out how the crystal quality or defect density has been altered by any growth step. Therefore, in this study, the effects of various growth steps on the defects in the GaSb epilayers grown on Si substrates are investigated comprehensively. With this aim in mind, GaSb epilayers grown on nominal Si substrates were subjected to different thermal treatments, SL layers were inserted in GaSb epilayers and the effect of vicinal Si substrates were examined. Structural analysis based on high-resolution x-ray diffraction (HR-XRD), scanning electron microscopy (SEM), cross-sectional scanning transmission electron microscopy (STEM) and atomic force

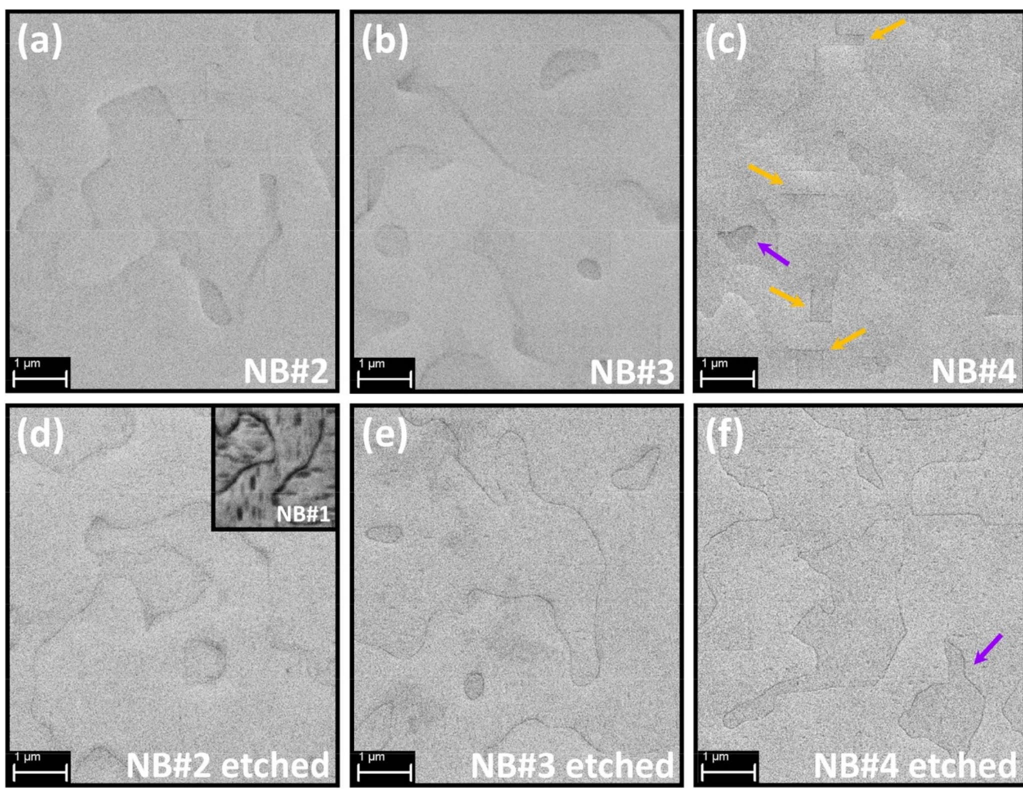

Figure 2. SEM images of as-grown and etched surfaces of (a)–(d) NB#2, (b)–(e) NB#3, and (c)–(f) NB#4, respectively. The inset in (d) shows the etched surface of the reference sample NB#1. The MTs and APBs are representatively marked by yellow and violet arrows, respectively, in (c) and (f).

microscopy (AFM) characterization techniques were systematically performed, and the results of the investigation were presented comparatively.

2. Methods

All samples were grown by using Veeco GEN20MC solid-source MBE system equipped with valved antimony (Sb), gallium (Ga) and aluminum (Al) dual filament cells. Sb_2 was used as group-V flux by keeping the cracker temperature at 900 °C. The beam equivalent pressure (BEP) was measured by an ionization gauge at the back of the substrate manipulator when it was rotated into the direct beam path. The base pressure of the MBE system was 7×10^{-11} Torr at the standby temperature of the effusion cells. The substrate temperature was monitored by using an IRCON pyrometer calibrated against the GaSb $(1 \times 3) \rightarrow (2 \times 5)$ surface reconstruction transition.

Undoped GaSb epilayers were grown on both nominal and vicinal Si(100) substrates with different miscut angles (Sil'tronix ST). For all the samples, the Ga flux was set to a BEP of 7.4×10^{-8} Torr, corresponding to a growth rate of 0.5 ML s^{-1}, and the group V/III BEP ratio was kept at 10. Prior to the growth, the Si substrates were loaded to the load-lock chamber and baked at 150 °C for 1 h under a minimum vacuum level of 1×10^{-7} Torr. After being transferred to the buffer chamber, each substrate was degassed at 400 °C by probing a minimum vacuum level of 2×10^{-8} Torr. In the growth chamber, the native oxide was desorbed from the Si substrate's surface at 850 °C, and the oxide removal process was verified by RHEED patterns. Following the oxide desorption, the temperature of the Si substrate was reduced to 530 °C and exposed to the Sb flux (BEP: 1.6×10^{-7} Torr) for 5 min prior to the GaSb growth.

For all GaSb epilayers containing AlSb NL, the Sb/Al BEP ratio was kept at 50 and the Al BEP was 6.2×10^{-9} Torr. The AlSb NL thickness of 20 ML was deposited with a growth rate of 0.1 ML s^{-1} at 485 °C on nominal/vicinal Si substrates. Then, the temperature was increased to 530 °C under Sb flux, and the Ga shutter was opened to start the growth of a 1 μm thick GaSb epilayer.

To investigate the effect of post-growth annealing on the crystal quality of GaSb epilayers, the samples were annealed at 570 °C for three different duration time (30, 60, and 120 min). In addition, two different thermal treatments were employed, whose further details are given below. During the annealing process, all samples were exposed to Sb flux (BEP: 7.8×10^{-7} Torr). The GaSb epilayers containing GaSb/AlSb SL layers with different number of periods were grown on nominal Si substrates to bend the dislocations and reduce the number of dislocations propagating towards the surface. For those samples, the SL growth rate was set to 0.5 ML s^{-1} for both GaSb and AlSb (the Al BEP was 6.6×10^{-8} Torr) and the thicknesses of the GaSb and AlSb layers were defined as 32 Å and 45 Å, respectively. To examine the influence

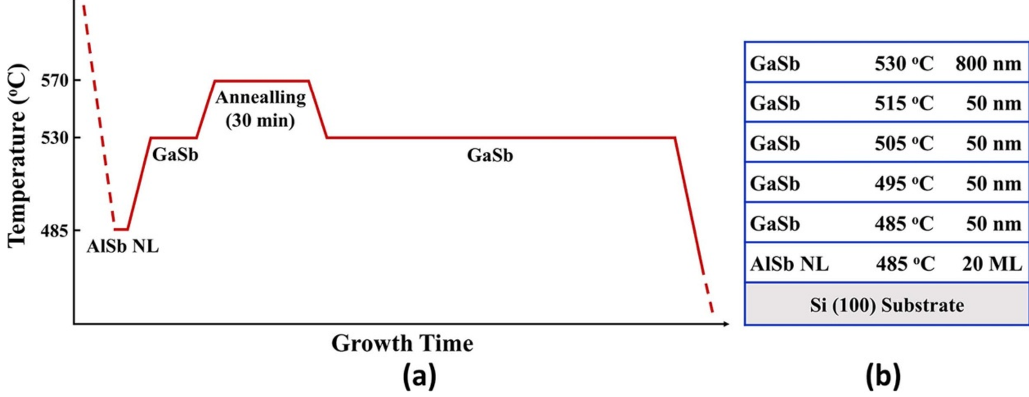

Figure 3. The growth steps of the samples (a) NB#5 and (b) NB#6.

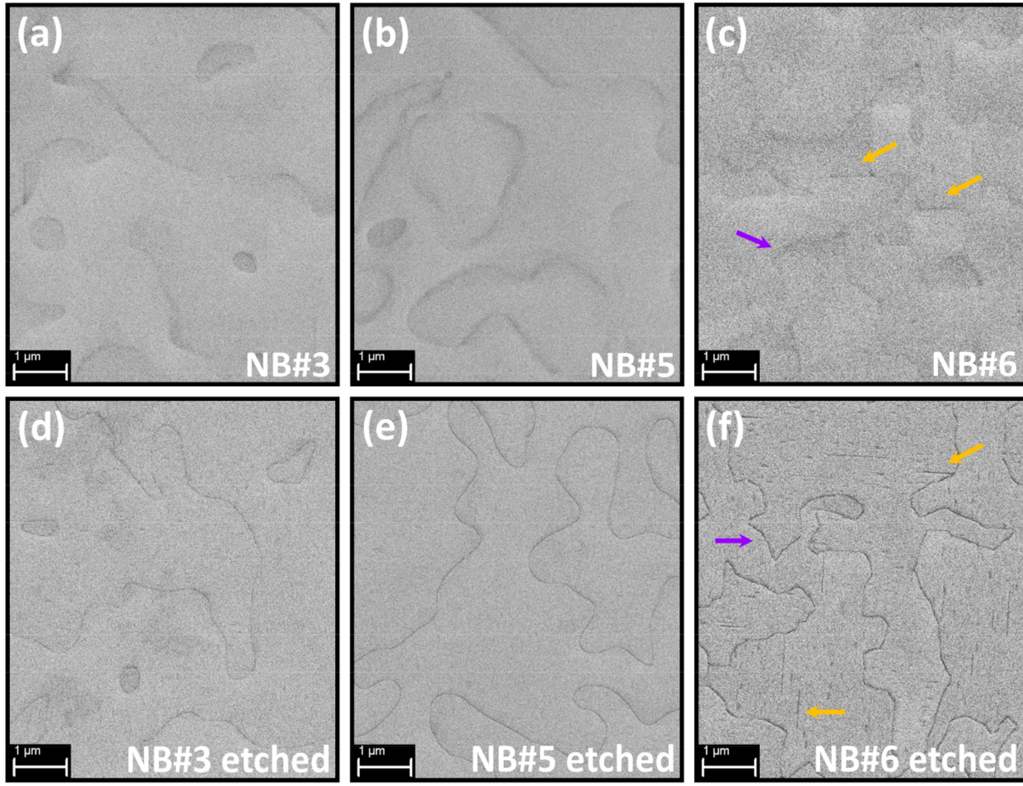

Figure 4. SEM images of the as-grown and etched surfaces of (a)–(d) NB#3, (b)–(e) NB#5, and (c)–(f) NB#6, respectively. The MTs and APBs are representatively marked by yellow and violet arrows, respectively, in (c) and (f).

of the misorientated substrates, the GaSb epilayers with 20 ML AlSb NL were grown on Si substrates with misorientation angles of 0.15°, 2°, 4°, and 6° towards [110] direction. For clearer overview, the growth parameters of all the samples are summarized in the supplementary data (table S1 (available online at https://stacks.iop.org/SST/36/025011/mmedia)).

Representative cross-sectional electron transparent specimens were prepared using a standard specimen preparation procedure that includes mechanical grinding, tripod wedge polishing and argon ion milling with a liquid nitrogen cooled stage. For argon-ion thinning, a precision ion polishing system (PIPS II, Model 695) was used at low temperatures. STEM images and energy-dispersive x-ray spectroscopy (EDS) spectra of the GaSb samples were taken with a JEOL ARM200CFEG TEM equipped with a probe C_s-corrector and a JEOL Centurio SDD detector. All images and spectra were collected using 200 kV accelerating voltage. The surface morphologies of the samples were investigated using a ZEISS model ULTRAplus field emission SEM.

In this study, $HCl:H_2O_2:H_2O$ (4:2:1) at 70 °C for 15 s was used as a defect sensitive solution to identify the APBs [18, 19]. After the etching process, SEM secondary electron (SE) images were obtained and the APB densities were determined by estimating the number of boundaries that cross

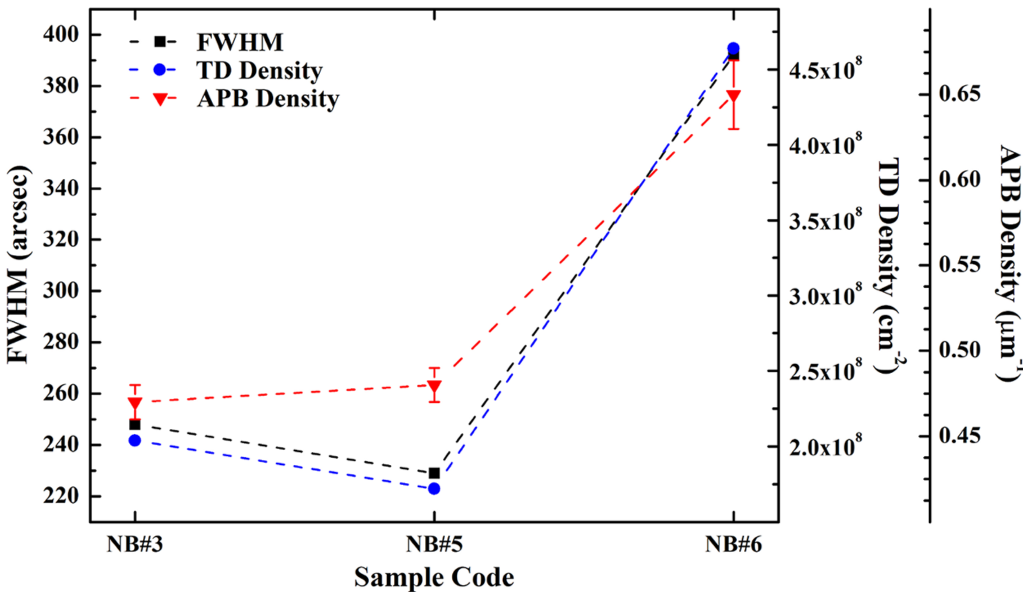

Figure 5. The FWHM of x-ray RC around the (004) reflection, the TD and APB densities of the samples, NB#3, NB#5, and NB#6. The dotted lines are guide for the eyes.

NB#7	
GaSb	725 nm
10 period GaSb/AlSb SL	77 nm
GaSb	200 nm
AlSb NL	20 ML
Si (100) Substrate	

NB#8	
GaSb	300 nm
165 period GaSb/AlSb SL	1270 nm
GaSb	200 nm
AlSb NL	20 ML
Si (100) Substrate	

NB#9	
GaSb	300 nm
20 period GaSb/AlSb SL	155 nm
GaSb	200 nm
20 period GaSb/AlSb SL	155 nm
AlSb	65 nm
20 period GaSb/AlSb SL	155 nm
AlSb	65 nm
20 period GaSb/AlSb SL	155 nm
AlSb	65 nm
20 period GaSb/AlSb SL	155 nm
GaSb	200 nm
AlSb NL	20 ML
Si (100) Substrate	

Figure 6. Detailed structures of the samples NB#7, NB#8, and NB#9.

along antiphase domains (APDs). For this purpose, we drew 11 lines along the [110] direction at equal intervals on the image and counted the numbers of boundaries crossing 12 μm in length and divided the number of boundaries by 12 μm [18, 20]. In order to have better statistics, we selected three different regions ($\sim$100 μm^2) on the etched sample and the APB density was computed by taking the average of the determined values.

The surface roughness of the GaSb samples was measured by NT-MDT NANOEDUCATOR II model AFM in semi-contact mode with an aluminum-coated silicon nitride tip of below 10 nm. The RMS values were obtained from areas of 100 μm^2.

HR-XRD rocking curve (RC) measurements were performed with a PANalytical X'Pert Pro MRD system equipped with a parabolic W/Si mirror, a four bounce (Ge220)

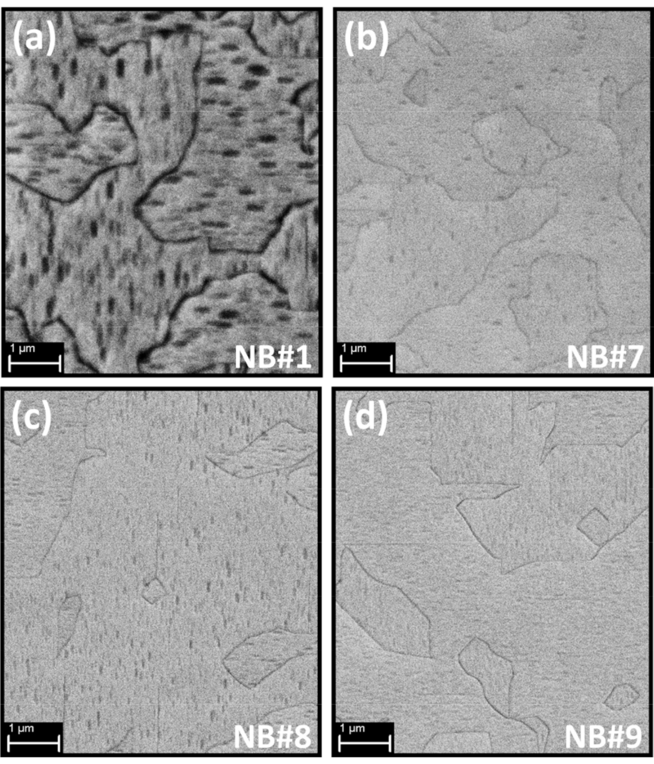

Figure 7. SEM images of etched samples; (a) NB#1, (b) NB#7, (c) NB#8, and (d) NB#9.

symmetric monochromator and a pixel detector using Cu $K_{\alpha 1}$ radiation ($\lambda = 0.15406$ nm). Omega RCs were measured via the symmetrical (004) GaSb reflection. The TD density of the samples were determined by using the x-ray RCs as described in [21].

3. Results and discussion

Our recent studies [18, 22] substantiated a greater efficiency of post-growth annealing compared to an increase in the growth temperature for GaSb epilayers grown on nominal Si substrates. Although the improvement in surface roughness was limited, the structural quality was improved by the post-growth annealing. In those studies, the GaSb epilayer grown at 530 °C with an AlSb NL thickness of 20 ML (NB#1) and post annealed at 570 °C for 30 min (NB#2) was selected as the one having the optimum performance in terms of the structural properties and surface roughness. The results obtained from our previous studies are summarized in table 1 [18, 22]. Since the optimized AlSb NL thickness was achieved by NB#1 having no additional growth steps, we use NB#1 as the reference sample in this study (otherwise indicated).

3.1. The effect of thermal annealing on GaSb epilayers

To investigate the optimum thermal treatment conditions, following the growth process, the GaSb epilayers were annealed for different durations at 570 °C. Additionally, two different thermal treatment processes were applied during the growth.

Figure 1 shows the variation of the FWHM values, the TD and APB densities depending on the post-annealing duration for the samples NB#1 (none), NB#2 (30 min), NB#3 (60 min), and NB#4 (120 min). It is clearly seen that the FWHM value, TD and APB densities decrease with increasing annealing duration up to 60 min (the sample NB#3) and then increase. The TD and APB densities of the sample NB#3 drops by 34% and 15%, respectively, compared to the reference sample (NB#1).

The surface morphologies of the as-grown and etched samples are comparatively investigated by SEM-SE imaging (figure 2). Thanks to the defect sensitive solution, the APBs are more pronounced on the etched surfaces. Either isolated single segments or connected segments in L-like shapes that are attributed to the MTs [23] pop out on the surface of NB#4, as presented in figure 2(c). In our previous study, it was shown that increasing the growth temperature or post-annealing at relatively higher temperatures result in a dramatic improvement in etch pits [18]. As can be seen in figures 2(d)–(f), the samples annealed at different durations exhibit similar behavior. On the other hand, the RMS roughness of the samples post-annealed for 30 min, 60 min, and 120 min are measured as 1.18, 1.22, and 1.26 nm, respectively (supplementary data figure S1). Those values are higher than the one obtained from the reference sample NB#1.

Now, we focus on the two different thermal treatments. The details of the growth processes of GaSb epilayers are displayed in figure 3. For NB#5, thermal annealing at 570 °C for 30 min was applied subsequent to the growth of 150 nm thick GaSb epilayer at 530 °C. Then the growth of GaSb epilayer at 530 °C was proceeded to reach the total thickness of 1 μm. For the sample NB#6, a 50 nm thick GaSb layer was grown at 485 °C following the initiation of 20 ML AlSb NL. The growth was subsequently carried on by deposition of 50 nm thick GaSb epilayers at different temperatures, as presented in figure 3(b). At this stage, the substrate temperature was changed with a very slow ramp rate (2.5 °C min^{-1}) so that a graded thermal annealing was conducted. After reaching the growth temperature of 530 °C, the growth process was completed by deposition of 800 nm thick GaSb epilayer.

The SEM-SE images of the as-grown and etched samples for NB#3, NB#5, and NB#6 are presented in figures 4(a)–(f), respectively. In this set, NB#3 is considered as a reference sample since it exhibits the lowest values in terms of RMS, TD and APB densities among the post-annealed samples. Although the post-annealed duration of NB#5 is less than the sample NB#3, no MTs are observed at the surface of this sample (figure 4(e)). On the other hand, NB#6 exhibits surficial MTs as well as APBs (figure 4(f)), indicating that the GaSb epilayer contains MTs reaching near the surface in the case of starting growth at lower temperatures. From figure 5, it reveals that the TD density of NB#5 is reduced by 16% compared to NB#3. On the contrary, the TD and APB densities of NB#6 are increased by 128% and 38%, respectively. In addition, the RMS value of NB#6 was determined as 2.26 nm (supplementary data figure S1), which is the highest value obtained within all the samples. Therefore, one can conclude that a higher amount of defects increases the surface roughness as well as degrades the surface quality. Based on above results,

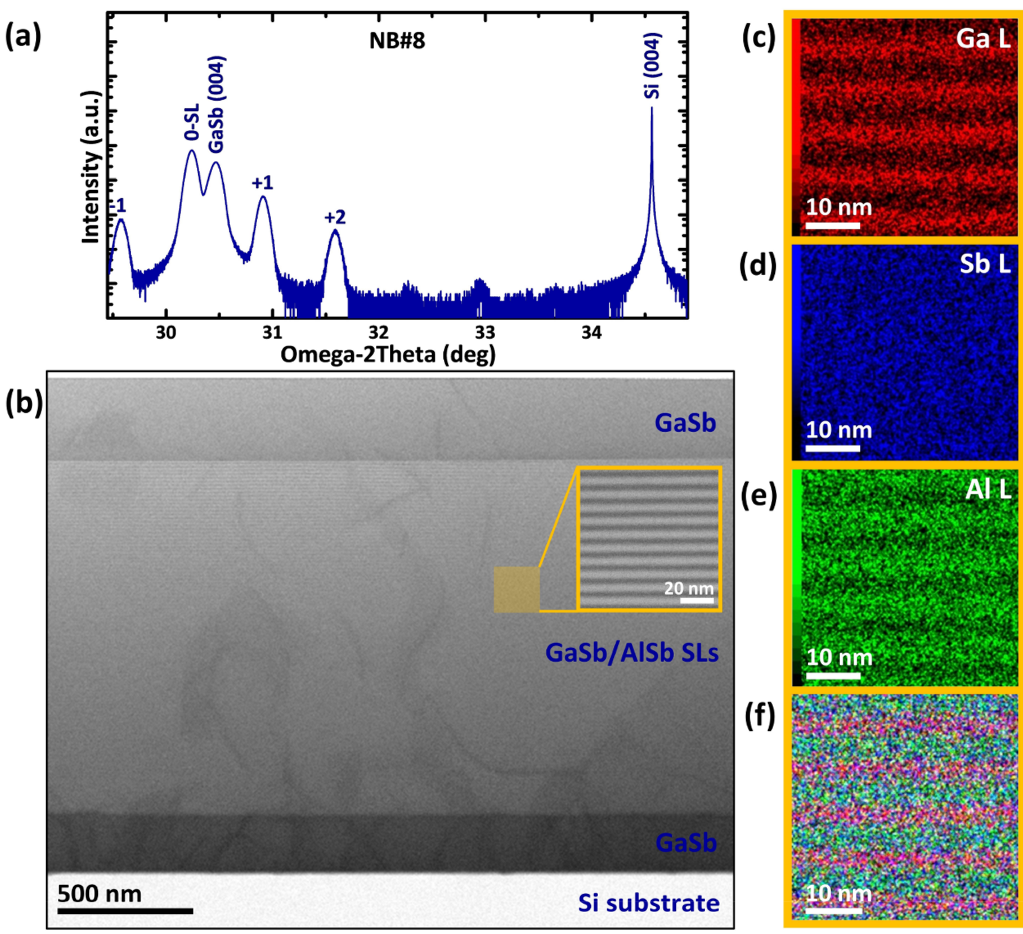

Figure 8. (a) HR-XRD pattern of NB#8 around the (004) reflection, (b) BF-STEM image of the entire structure. The inset shows a high magnification image of the area highlighted by the orange square and the corresponding EDS elemental maps, (c) Ga L, (d) Sb L, (e) Al L, and (f) the overlay of all the elements.

the annealing treatment at the intermediate step is found to be a more promising method than the graded thermal annealing.

Comparing NB#5 with NB#2, which is post-annealed for the same duration, an enhancement of the entire crystal quality of the GaSb epilayer is in any case apparent, which indicates a more effective method. However, contrary to the improvement in structural quality, the surface roughness was deteriorated to 1.84 nm for the sample NB#5 as can be seen from figure S1.

3.2. The growth of GaSb epilayers with superlattice layers

Using the unique capabilities of MBE, we design GaSb-AlSb/GaSb SL-GaSb multilayers in order to study the influence of GaSb/AlSb SLs on the quality of GaSb epilayers. Figure 6 presents the structures of GaSb epilayers with GaSb/AlSb SL layers. The main difference between the samples is the period number and the position of SL layers within the epilayer. For NB#8 and NB#9, the thickness of buffer layers inevitably exceeds 1 μm to examine the effect of the number of SL period. However, the overall thickness of GaSb epilayers were fixed in all the samples to 1 μm.

The surface morphology is studied via AFM, which revealed no distinct difference between the reference sample NB#1 and the SL inserted samples. The surface roughness of the samples NB#1, NB#7, NB#8, and NB#9 is determined as 1.06, 1.13, 0.90, and 0.90 nm, respectively (supplementary data figure S2). The SEM-SE images of the etched samples in this set are presented in figure 7. From those images, the APB densities were calculated as 0.56, 0.33, and 0.44 μm^{-1} for NB#7, NB#8, and NB#9, respectively. Comparing those values with 0.55 μm^{-1}, which is obtained for NB#1, we see that NB#7 has almost the same value and with the dramatic increase in the number of SL period number, the APB densities of NB#8 and NB#9 are decreased by 41% and 21%, respectively. Thus, the obtained values indicate that the APB density changes depending on the number of SL period. Nevertheless, all of the samples contain etch pits with various sizes depending on the SL period number and position inserted in GaSb epilayer. As can be seen from figure 7(d), the size of etch pits in NB#9 are significantly small compared to the other samples in this set. Thereby, we concluded that the number and position of SL layers in GaSb has a major impact on the reduction of the APB density and the size of etch pits.

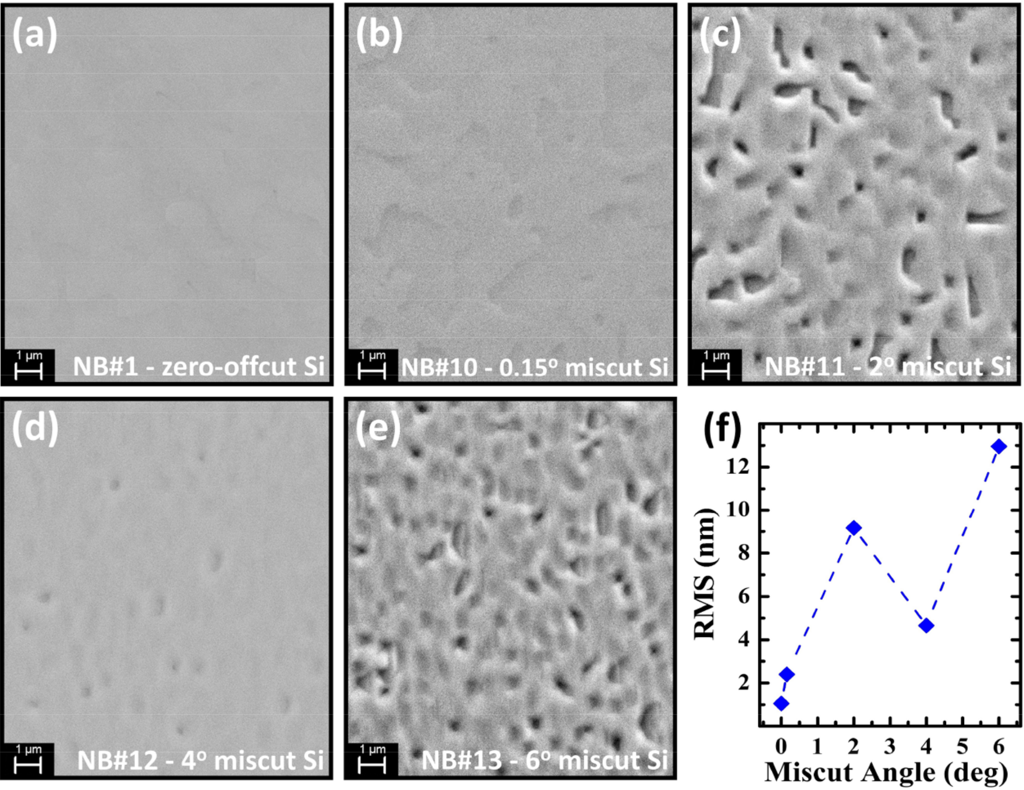

Figure 9. SEM images of (a) NB#1 as the reference sample and GaSb epilayers grown on Si(100) substrates with misorientation angles of (b) 0.15°, (c) 2°, (d) 4°, and (e) 6° towards [110] direction. (f) RMS roughness of the GaSb epilayers as a function of miscut angle.

For the sample NB#8, the XRD pattern and bright field (BF) STEM images with related EDS elemental maps are presented in figure 8. The fringes having a spacing of 7.7 nm in figure 8(a) and uniform elemental distribution maps in figures 8(c)–(f) extracted from the SL region in figure 8(b) denote successfully grown GaSb with GaSb(32 Å)/AlSb(45 Å) SLs. Looking at the entire structure of NB#8 in figure 8(b), it is clearly seen that the defect density is reduced with the beginning of SLs and is gradually decreased throughout the SL layer. This observation confirms that SLs region acts as a defect filter. Even though the defects reaching the surface is inevitable, it is noteworthy that they are substantially diminished.

3.3. The role of vicinal substrate on GaSb epilayers

In order to study the influence of the vicinal substrate on the crystal quality of GaSb epilayer, we compare the vicinal and nominal substrates. The Si(100) substrates with misorientation angles of 0.15°, 2°, 4°, and 6° towards [110] direction were used in this set, which refers to the samples NB#10, NB#11, NB#12, NB#13, respectively. Figure 9 represents the SEM images of the as-grown GaSb epilayers on vicinal Si substrates. Unlike the other samples, the features defining APBs and MTs were not observed on the surface of as-grown samples. A change in the surface morphology and a non-monotonic behavior in the surface roughness was observed depending on the miscut angle of Si substrate. The surface roughness of the samples are determined as 2.40, 9.17, 4.66, and 12.95 nm for NB#10, NB#11, NB#12, NB#13, respectively. The NB#10 grown on vicinal Si surface with low miscut angle (0.15°) results in a similar surface morphology of the reference sample NB#1 grown on nominal Si substrate (figures 9(a) and (b)). Whereas the GaSb epilayers grown on vicinal Si substrate with miscut angles of 2° and 6° possess significantly rougher surfaces (figure 9(f)), a smoother surface was obtained for the one grown on 4° miscut Si substrate. The sample grown on the lowest angle miscut Si substrate exhibits the smoothest surface morphology with the lowest surface roughness. On the other hand, the surface roughnesses of all the GaSb epilayers grown on vicinal substrates are larger compared to the reference sample NB#1.

The SEM-SE images in figure 10 display a considerable variation in the APB density and the APD size. As expected, the use of vicinal Si substrates resulted in the suppression of APDs and consequently, the APDs appear in the form with significant closed-loop boundaries in the case of using vicinal Si(100) substrates with high miscut angles (2°–6°). Among those, the APB density dramatically decreases down to a value of 0.06 μm^{-1}, for the sample NB#12 grown on 4° miscut Si substrate (figure 10(d)). Thus, by virtue of using the miscut Si substrates, most probably the self-annihilation of APBs were occurred during the growth [24].

Moreover, the best FWHM value and the lowest TD density are found as 259 arcsec and 1.98×10^8 cm^{-1}, respectively, for the sample grown on 4° miscut Si substrate (figure 11). When compared to the reference sample NB#1 grown on nominal substrate, the TD and the APB density is reduced by 36% and

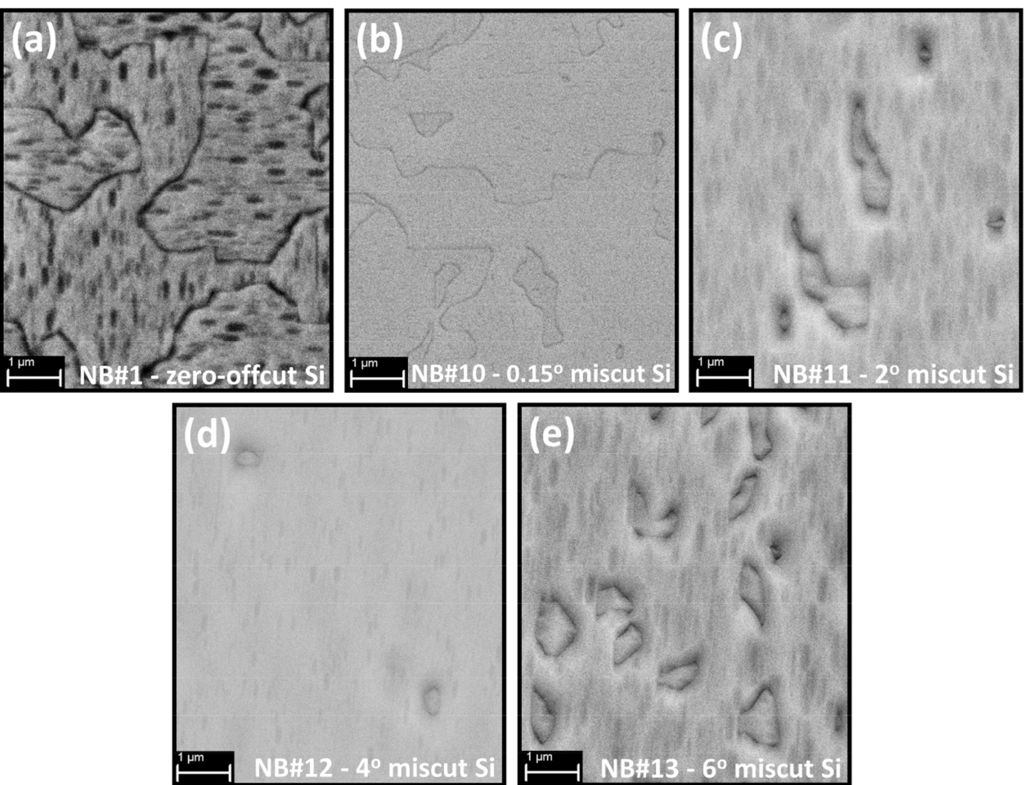

Figure 10. SEM images of (a) etched NB#1 as the reference sample and etched GaSb epilayers grown on Si(100) substrates with misorientation angles of (b) 0.15°, (c) 2°, (d) 4°, and (e) 6° towards [110] direction.

89%, respectively, underlining the significance of the choice of the miscut angle.

3.4. Summary

In consideration of all results achieved in this study, a GaSb epilayer surface is produced without etch pits as a result of thermal annealing. The results indicate that thermal annealing at the beginning of the growth is a more effective procedure than a post-growth annealing treatment. Table 2 summarizes the results obtained from the samples subjected to different heat treatments. For NB#5, a MT free surface was obtained and the lowest TD density was achieved compared to the other samples. Comparing NB#5 with NB#3, which is the sample post-annealed for 60 min, shows that an intermediate annealing step does not have a dramatic influence on the APB density. However, it is believed that this process can be improved by adjusting the annealing duration or step runs. Regarding the surface morphology, a rougher surface is obtained for NB#6, which is consistent with a higher amount of TD and APB densities. It is known that the post annealed samples have APDs with sharp boundaries [18]. This effect is more pronounced in the case of the intermediate annealing treatment, which could be the reason for the increase in RMS roughness.

It is confirmed that the sample NB#8 is a more functional design among the samples with GaSb/AlSb SLs. Although the total thicknesses of the samples NB#8 and NB#9 are similar, a higher number of SL period reduces the APB density significantly without surface roughness degradation. Nevertheless, the etch pits still appear on the surface. For the sample NB#8, it was possible to reduce the APB density down to 0.3 μm^{-1} range that is close to the ones obtained for the samples grown on vicinal substrates excluding the one having 4° miscut angle. Besides, a smoother surface with 0.90 nm RMS roughness is achieved compared to the samples grown on vicinal Si substrates. As mentioned before, the SL layers in the GaSb epilayer act as a dislocation filter by preventing the defects to propagate towards the surface. However, in terms of defects, using a Si vicinal substrate may be more advantageous regarding the time and material consumption, if the surface morphology is not crucial.

MTs are not observed and closed-loop boundaries appear on the surface of the samples grown on vicinal substrates. It is possible that the closed-loop boundaries are due to the annihilation of the APDs, although this should be confirmed in future studies. The obtained results are summarized in table 3. Among the vicinal substrates, Si(100) substrate with 4° miscut angle provides the suppression of APBs in a considerable extent. However, as depicted from the AFM images (supplementary data figure S3), the surface roughness is severely increased, which may particularly affect the performance of SL device structures grown on such rough buffer epilayers.

The vicinal Si substrates with low miscut angles exhibit a single height type surface configuration. As the miscut angle is increased, a surface with two-step configuration mostly occurs [25], and the double-step height type can facilitate the suppression of APDs. For this reason, the abrupt change of the APB density between the samples hinges on the miscut angle of the vicinal Si substrates. As illustrated in figure 12, the

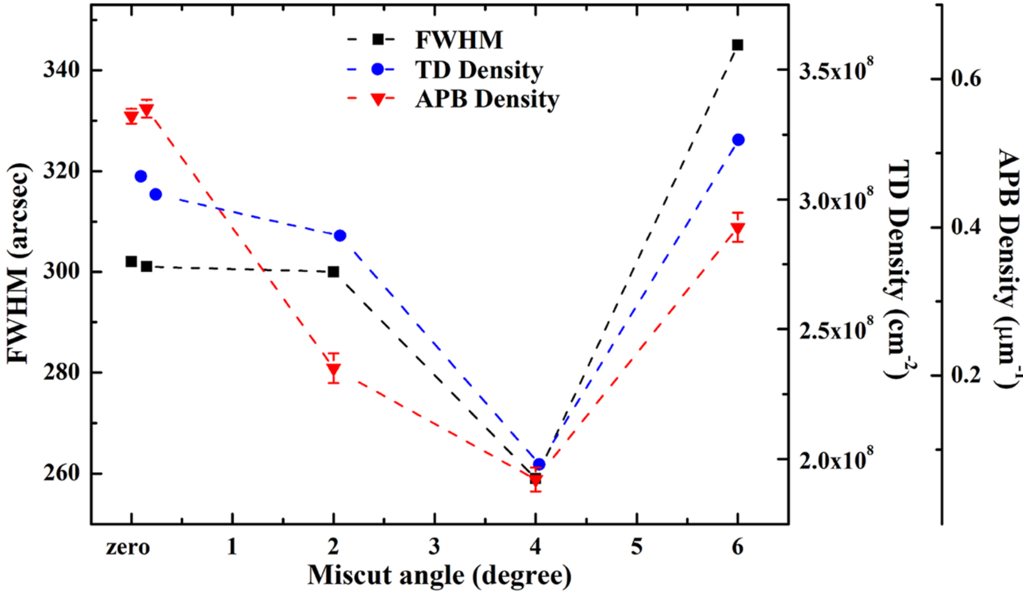

Figure 11. The FWHM of x-ray RC around the (004) reflection, the TD and APB densities of the samples having miscut angles of 0.15°, 2°, 4°, and 6°, which correspond to the samples NB#10, NB#11, NB#12, and NB#13, respectively. The dotted lines are guide for the eyes.

Table 2. The obtained results from the samples subjected to various thermal treatment processes.

Sample code	NB#1[a]	NB#2	NB#3	NB#4	NB#5	NB#6
RC FWHM (arcsec)	302	260	248	288	229	392
TD density (cm^{-2})	3.09×10^8	2.36×10^8	2.04×10^8	2.88×10^8	1.72×10^8	4.64×10^8
The APB density (μm^{-1})	0.55	0.53	0.47	0.58	0.48	0.65
RMS (nm)	1.06	1.20	1.22	1.06	1.84	2.26

[a] Reference sample.

Table 3. The obtained results from the samples grown on vicinal Si(100) substrates with different miscut angles.

Sample code	NB#1[a]	NB#10	NB#11	NB#12	NB#13
Miscut angle (degree)	0	0.15	2	4	6
RC FWHM (arcsec)	302	301	300	259	345
TD density (cm^{-2})	3.09×10^8	3.02×10^8	2.86×10^8	1.98×10^8	3.23×10^8
APB density (μm^{-1})	0.55	0.56	0.21	0.06	0.40
RMS (nm)	1.06	2.40	9.17	4.66	12.95

[a] Reference sample.

miscut angle (θ) of the vicinal substrates alters the step length (L) and the density of the steps. Increasing the miscut angle reduces the step length and increases the density of the steps. It is known that the AlSb NL generates interfacial misfit (IMF) dislocations along the interface [26]. Therefore, the APB density variation between the vicinal Si substrates is attributed to the relation between the step length and IMF array spacing. If the step length is significantly shorter or longer than the IMF array spacing, the number of interaction points between the step edge and the IMF dislocations will increase, resulting in rather large defect density [10]. In our case, the APB density decreases with increasing miscut angle up to 4° but this trend changes for further increase in the miscut angle. This behavior could be related with the fixed AlSb NL thickness (20 ML) used in this study but it should be confirmed with further studies.

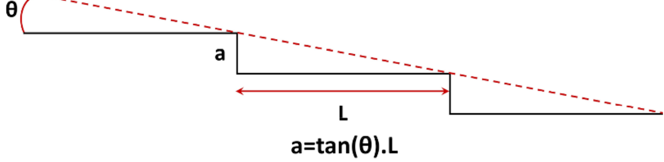

Figure 12. Step geometry of the vicinal Si(100) substrate.

Consequently, the crystal quality of GaSb epilayers can be improved using vicinal Si substrates with SLs as dislocation filters or by thermal annealing. These results strongly point out that the growth process can be diversified via combinations of such methods. This also means that the growth of high quality GaSb epilayers on Si to be used as a virtual substrate instead of GaSb still needs further attention.

4. Conclusion

We have devised an easy and efficient procedure to reveal the defects in GaSb epilayers grown on nominal/vicinal Si substrates. The defect sensitive solution that we used enables us to compare the defects created in GaSb epilayers. In addition, we present a comparative investigation of highly mismatched GaSb epilayers grown on Si substrates grown by various growth steps. The findings reveal that the particular growth process for lessening different types of defects within the epilayer is crucial for the monolithic growth of GaSb on Si. Even though the crystal quality of GaSb on Si is significantly enhanced by applying various growth steps, our results demonstrate that there is still room for the improvement of buffer layers with high crystal quality. Obviously, the growth conditions should be optimized by applying a combination of more than one method. The overall results suggest that future research should concentrate on the investigation of new approaches for developing a better GaSb/Si interface layer.

Acknowledgments

This study was supported in part by the Scientific and Technological Research Council of Turkey (TÜBİTAK) under the Grant No. 116F199 and by Eskişehir Technical University under the Project No. BAP-1305F092. This study has received funding from the European Union's Horizon 2020 research and innovation programme under Grant Agreement No. 823717–ESTEEM3. The authors thank Marion Kelsch for TEM specimen preparation.

ORCID iDs

Burcu Arpapay https://orcid.org/0000-0002-0784-560X
Y Eren Suyolcu https://orcid.org/0000-0003-0988-5194
Peter A van Aken https://orcid.org/0000-0003-1890-1256
Uğur Serincan https://orcid.org/0000-0002-6305-4343

References

[1] Feifel M *et al* 2018 Direct growth of III–V/silicon triple-junction solar cells with 19.7% efficiency *IEEE J. Photovolt.* **8** 1590–5
[2] Sun K, Jung D, Shang C, Liu A, Morgan J, Zang J, Li Q, Klamkin J, Bowers J E and Beling A 2018 Low dark current III–V on silicon photodiodes by heteroepitaxy *Opt. Express* **26** 13605–17
[3] Tang M, Park J-S, Wang Z, Chen S, Jurczak P, Seeds A and Liu H 2019 Integration of III–V lasers on Si for Si photonics *Prog. Quantum Electron.* **66** 1–18
[4] Razeghi M, Haddadi A, Hoang A M, Huang E K, Chen G, Bogdanov S, Darvish S R, Callewaert F and McClintock R 2013 Advances in antimonide-based type-II superlattices for infrared detection and imaging at center for quantum devices *Infrared Phys. Technol.* **59** 41–52
[5] Hosseini Vajargah S, Ghanad-Tavakoli S, Preston J S, Kleiman R N and Botton G A 2013 Growth mechanisms of GaSb heteroepitaxial films on Si with an AlSb buffer layer *J. Appl. Phys.* **114** 113101
[6] Deng Z, Guo D, Burguete C G, Xie Z, Huang J, Liu H, Wu J and Chen B 2019 Demonstration of Si based InAs/GaSb type-II superlattice p-i-n photodetector *Infrared Phys. Technol.* **101** 133–7
[7] Delli E *et al* 2019 Mid-infrared InAs/InAsSb superlattice nBn photodetector monolithically integrated onto silicon *ACS Photon.* **6** 538–44
[8] Durlin Q, Perez J P, Cerutti L, Rodriguez J B, Cerba T, Baron T, Tourniè E and Christol P 2019 Midwave infrared barrier detector based on Ga-free InAs/InAsSb type-II superlattice grown by molecular beam epitaxy on Si substrate *Infrared Phys. Technol.* **96** 39–43
[9] Akahane K, Yamamoto N, Gozu S and Ohtani N 2004 Heteroepitaxial growth of GaSb on Si(001) substrates *J. Cryst. Growth* **264** 21–25
[10] Huang S H, Balakrishnan G, Khoshakhlagh A, Dawson L R and Huffaker D L 2008 Simultaneous interfacial misfit array formation and antiphase domain suppression on miscut silicon substrate *Appl. Phys. Lett.* **93** 071102
[11] Noh Y K, Kim M D, Oh J E and Yang W C 2010 Structural and optical properties of GaSb films grown on AlSb/Si (100) by insertion of a thin GaSb interlayer grown at a low temperature *J. Korean Phys. Soc.* **57** 173–7
[12] Craig A P, Carrington P J, Liu H and Marshall A R J 2016 Characterization of 6.1 Å III–V materials grown on GaAs and Si: a comparison of GaSb/GaAs epitaxy and GaSb/AlSb/Si epitaxy *J. Cryst. Growth* **435** 56–61
[13] Rodriquez J-B, Madiomanana K, Cerutti L, Castellano A and Tournié E 2016 X-ray diffraction study of GaSb grown by molecular beam epitaxy on silicon substrates *J. Cryst. Growth* **439** 33–39
[14] Gutiérrez M, Lloret F, Jurczak P, Wu J, Liu H Y and Araújo D 2018 GaSb and GaSb/AlSb superlattice buffer layers for high-quality photodiodes grown on commercial GaAs and Si substrates *J. Electron. Mater.* **47** 5083–6
[15] Georgakilas A, Papavassiliou C, Constantinidis G, Tsagaraki K, Krasny H, Löchtermann E and Panayotatos P 1992 Effects of Si(100) tilting angle and prelayer conditions on GaAs/Si heterostructures *Appl. Surf. Sci.* **102** 67–72
[16] Yamaguchi M 1991 Dislocation density reduction in heteroepitaxial III–V compound films on Si substrates for optical devices *J. Mater. Res.* **6** 376–84
[17] Ayers J E, Schowalter L J and Ghandhi S K 1992 Post-growth thermal annealing of GaAs on Si(001) grown by organometallic vapor phase epitaxy *J. Cryst. Growth* **125** 329–35
[18] Arpapay B and Serincan U 2020 The role of antiphase domain boundary density on the surface roughness of GaSb epilayers grown on Si (001) substrates *Superlattices Microstruct.* **140** 106450
[19] Reijnen L, Brunton R and Grant I R 2005 GaSb single-crystal growth by vertical gradient freeze *J. Cryst. Growth* **275** e595–e600
[20] Naresh-Kumar G, Vilalta-Clemente A, Jussila H, Winkelmann A, Nolze G, Vespucci S, Nagarajan S, Wilkinson A J and Trager-Cowan C 2017 Quantitative imaging of anti-phase domains by polarity sensitive orientation mapping using electron backscatter diffraction *Sci. Rep.* **7** 10916
[21] Ayers J E 1994 The measurement of threading dislocation densities in semiconductor crystals by x-ray diffraction *J. Cryst. Growth* **135** 71–77
[22] Serincan U and Arpapay B 2019 Structural and optical characterization of GaSb on Si (001) grown by molecular beam epitaxy *Semicond. Sci. Technol.* **34** 035013
[23] Rodriguez J-B, Cerutti L, Patriarche G, Largeau L, Madiomanana K and Tournié E 2017 Characterization of antimonide based material grown by molecular epitaxy on vicinal silicon substrates via a low temperature AlSb nucleation layer *J. Cryst. Growth* **477** 65–71

[24] Ueda O, Soga T, Jimbo T and Umeno M 1989 Direct evidence for self-annihilation of antiphase domains in GaAs/Si heterostructures *Appl. Phys. Lett.* **55** 445–7

[25] Barbier L, Khater A, Salanon B and Lapujoulade J 1991 Observation of the double-step-single-step transition on a vicinal surface of Si(100) *Phys. Rev.* B **43** 14730–3

[26] Hosseini Vajargah S, Couillard M, Cui K, Ghanad Tavakoli S, Robinson B, Kleiman R N, Preston J S and Botton G A 2011 Strain relief and AlSb buffer layer morphology in GaSb heteroepitaxial films grown on Si as revealed by high-angle annular dark-field scanning transmission electron microscopy *Appl. Phys. Lett.* **98** 082113